Available online at www.sciencedirect.com

ScienceDirect

IFAC PapersOnLine 56-2 (2023) 2701–2706

Minimum-Variance Model Predictive Control for Dual Fluidized Bed Circulation Control

Lukas Stanger * **Alexander Schirrer** * **Alexander Bartik** ** **Martin Kozek** *

* *TU Wien, Institute of Mechanics and Mechatronics, Getreidemarkt 9, 1060 Vienna, Austria (e-mail: {lukas.stanger,alexander.schirrer,martin.kozek}@tuwien.ac.at)*

** *TU Wien, Institute of Chemical, Environmental and Bioscience Engineering, Getreidemarkt 9, 1060 Vienna, Austria (e-mail: alexander.bartik@tuwien.ac.at)*

Abstract: Dual fluidized bed steam gasification enables the production of gaseous energy carriers from woody biomass or biogenic residues. The circulation of bed material in dual fluidized bed gasifiers strongly affects the process behavior. Therefore, precise control of the bed material circulation is desired. This paper presents a control algorithm addressing two aspects of the given problem setting: On the one hand, redundant control actuators are available. Typically, there are several air streams to the reactors influencing the bed material circulation. On the other hand, only black box models with uncertainties in their model parameters are available for model-based control design. The presented control algorithm uses a model predictive controller considering known uncertainties in the model parameters and drives the process in a region with the lowest model uncertainties. This results in an improvement of the closed-loop performance when the actual plant deviates from the internal model used for the model predictive control predictions. Simulations show 66 % less offset from the design trajectory with the presented algorithm when compared to a standard model predictive controller.

Keywords: Model predictive and optimization-based control, Process control applications, Model uncertainties, Control allocation, Dual fluidized bed gasification

1. INTRODUCTION

Dual Fluidized Bed (DFB) steam gasification can be used to produce high-quality product gas from woody biomass or biogenic residues (Benedikt et al. (2018)). For an efficient operation of DFB plants, process variables such as reactor temperatures, product gas mass flow or product gas quality have to be controlled. Typically, a combination of single-input single-output controllers is used to control these process variables, as presented in Nigitz et al. (2020) and Pröll and Hofbauer (2010). Multiple-input multiple-output control concepts cannot be found in the literature for DFB plants, yet offer the chance to increase process efficiency (Stanger et al. (2023)). To control the reactor temperatures or the product gas quality, effective control of the bed material circulating between the two reactors is required since the bed material is transporting both heat and char between the reactors. The bed material circulation in DFB gasifiers is modeled mostly based on computational fluid dynamics and is shown in Liu et al. (2016) or Kraft et al. (2017). Estimating the mass of bed material circulating in fluidized beds is a challenging task and discussed for example in Medrano et al. (2016) and Matsuda (2008). In Stollhof et al. (2018) and Fuchs et al. (2018) it is shown, that the pressure gradient in the upper part of the combustion reactor (CR) is a reliable indicator for the bed material circulation. The bed material circulation is mainly manipulated by the air streams to the CR: There are air inlets at different reactor heights. Thus, by changes in the air staging, the circulation can be influenced. At the advanced 100 kW DFB pilot plant at TU Wien, three air stages are available at the CR. Therefore, more control actuators are available than variables that need to be controlled.

In process control, split range control is often applied when redundant control actuators are available, as presented in Fonseca et al. (2013) and Reyes-Lúa and Skogestad (2020). In motion control for vehicles and aircrafts, control allocation is applied for over-actuated systems. In Johansen and Fossen (2013) a survey of control allocation algorithms is given and different applications are discussed. A method for control allocation incorporating the information on model uncertainties is presented in Grauer and Pei (2021).

The scope of this work is to present a method on how to handle the availability of redundant control actuators by using the knowledge about model uncertainties. The algorithm leads to the usage of the control actuators in a way that the process is driven within a region of low model uncertainties. The control algorithm is presented

⋆ This work was supported by the project ADORe-SNG, which is funded by the Austrian Climate and Energy Fund (FFG, No.881135).

10.1016/j.ifacol.2023.10.1364

within a model predictive control (MPC) framework which allows the explicit consideration of input constraints, since constraints often occur in process control problems. Simulations are shown for the cold flow model (CFM) of the advanced 100 kW DFB pilot plant at TU Wien and demonstrate the effectiveness of the proposed algorithm.

2. PROCESS DESCRIPTION

The main components of a DFB gasifier are the gasification reactor (GR) and the combustion reactor (CR). Both reactors are operated as fluidized bed reactors, the GR as a bubbling fluidized bed reactor and the CR as a fast fluidized bed reactor. These two reactors are connected by loop seals. Bed material is constantly circulating between the GR and the CR transporting ungasified fuel from the GR to the CR and heat from the CR to the GR. The amount of heat and ungasified fuel transported between the two reactors depends on the bed material circulation rate (Stollhof et al. (2018)).

2.1 Cold Flow Model of a Dual Fluidized Bed Gasifier

CFMs have been widely used to investigate the fluid dynamical behavior of DFB gasifiers (Shrestha et al. (2016)). In this paper, modeling and control design are based on the CFM at TU Wien, since experiments can be easier carried out at the CFM. Fig. 1 shows the design of the CFM. A detailed description of the experimental setup can be found in Lunzer et al. (2021) and Fuchs (2013).

The CFM at TU Wien is designed in a way that the dimensionless similarity is given to the hot 100 kW pilot plant, which means that dimensionless quantities such as Reynolds number or Archimedes number are similar. Therefore, it behaves similarly in terms of fluid dynamics. The reactors and the loop seals of the CFM are fluidized with air, and bronze particles are used as bed material. Whereas the 100 kW pilot plant has three air inlets to the CR, there are only two air stages available at CFM: Primary air and secondary air. Those are the most significant inputs to manipulate the bed material circulation. The pressure is measured at various positions in both reactors and in the loop seals. For this work, the pressure measurements in the upper part of the CR are relevant and used for control, whereby the pressure difference is denoted as Δp.

2.2 Plant Model

In steady state, the pressure difference Δp in the upper part of the combustion reactor is modeled by the linear relationship

$$\Delta p = b_0 + b_1 \dot{V}_p + b_2 \dot{V}_s, \tag{1}$$

where $\dot{V}_p$ and $\dot{V}_s$ are the primary and secondary air flows, respectively. With the input vector

$$\boldsymbol{u} = \begin{bmatrix} 1 & \dot{V}_p & \dot{V}_s \end{bmatrix}^T = \begin{bmatrix} 1 & u_1 & u_2 \end{bmatrix}^T, \tag{2}$$

and the parameter vector

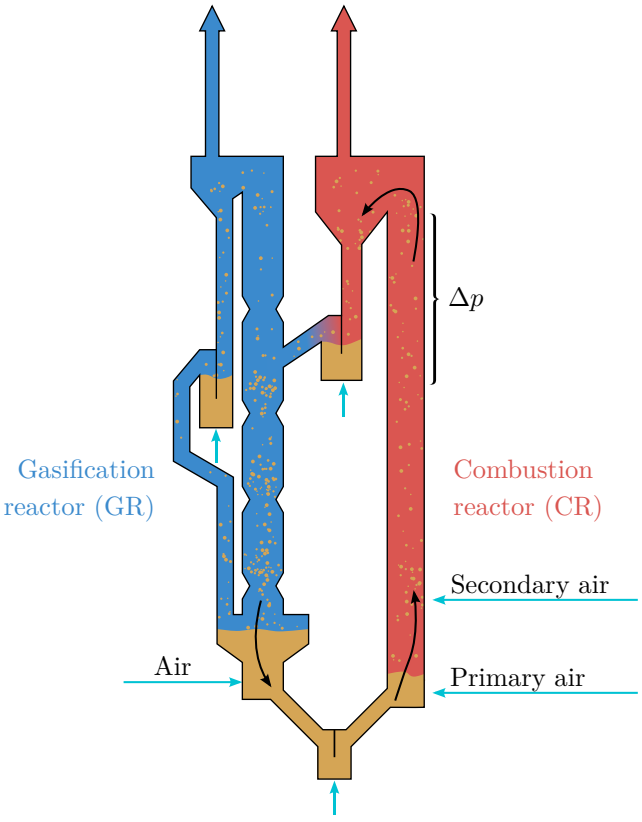

Fig. 1. Cold Flow Model to investigate the fluid dynamical behavior of the advanced 100 kW DFB pilot plant at TU Wien.

$$\boldsymbol{\theta} = \begin{bmatrix} b_0 & b_1 & b_2 \end{bmatrix}^T \tag{3}$$

we can write (1) compact to

$$\Delta p = \boldsymbol{u}^T \boldsymbol{\theta}. \tag{4}$$

The pressure difference Δp corresponds to the system state x. The parameter vector $\boldsymbol{\theta}$ is estimated from measurement data. Moreover, the parameter covariance matrix $\boldsymbol{\Sigma}$ is estimated from measurement data and is later used for control design.

If an input variable is changed step-wise, a PT1-like response can be observed in the pressure difference. This dynamic behavior is modeled by the first order differential equation

$$\dot{x} = \frac{1}{\tau}\big(-x + b_0 + b_1 u_1 + b_2 u_2 \big) \tag{5}$$

with the time constant τ.

3. METHODS

In this section, first, the procedure of the control algorithm is described. Then, the disturbance model and the observer design are presented, followed by the minimum-variance MPC (MV-MPC) approach proposed as the main contribution.

3.1 Algorithmic Procedure

At each time step k, the following steps are carried out

(1) *Observer*: Both the model state and a disturbance state are estimated by a Kalman filter.
(2) *Target Calculation*: An operating point is calculated considering the disturbance state. This operating point is then tracked by the MPC.
(3) *Solution of the MPC optimization problem*: The optimal sequence of control inputs is calculated by solving the MPC optimization problem.

3.2 Observer Design

In order to capture the plant-model mismatch and unmeasured disturbances the plant model is augmented by a disturbance model as follows:

$$\begin{cases} \dot{x} = \frac{1}{\tau}\big(-x + b_0 + b_1 u_1 + b_2 u_2 + d\big) \\ \dot{d} = 0 \\ y = x, \end{cases} \tag{6}$$

with the disturbance state d. This disturbance state models process variables that are influencing the bed material circulation and are slowly changing over time, such as the total amount of bed material in the system. A discretization of the model leads to the state-space system

$$\begin{aligned} \begin{bmatrix} x_{k+1} \\ d_{k+1} \end{bmatrix} &= \begin{bmatrix} a & b_d \\ 0 & 1 \end{bmatrix} \begin{bmatrix} x_k \\ d_k \end{bmatrix} + \begin{bmatrix} \boldsymbol{b} \\ \boldsymbol{0} \end{bmatrix} \boldsymbol{u}_k, \\ y_k &= x_k, \end{aligned} \tag{7}$$

where the entries a, b_d, and $\boldsymbol{b}$ in the system matrices are both a function of the continuous-time parameters and the sampling time.

A Kalman filter is designed to estimate both the original state x and the disturbance state d:

$$\begin{aligned} \begin{bmatrix} \hat{x}_{k+1} \\ \hat{d}_{k+1} \end{bmatrix} &= \begin{bmatrix} a & b_d \\ 0 & 1 \end{bmatrix} \begin{bmatrix} \hat{x}_k \\ \hat{d}_k \end{bmatrix} + \begin{bmatrix} \boldsymbol{b} \\ \boldsymbol{0} \end{bmatrix} \boldsymbol{u}_k \\ &\quad + \begin{bmatrix} l_x \\ l_d \end{bmatrix} (-y_{m|k} + \hat{x}_k), \\ \hat{y}_k &= \hat{x}_k, \end{aligned} \tag{8}$$

with the Kalman gain matrix $\boldsymbol{L} = [l_x \, l_d]^T$ and the measured output variable y_m.

3.3 MPC Cost Function

The MPC is designed to track a constant reference for the output y. A quadratic cost function is formulated and is minimized at every time step k:

$$\begin{aligned} \min_{\boldsymbol{U}} J_{\text{MPC}} = \sum_{i=0}^{N-1} &(x_{k+i} - \bar{x}_k)^T q (x_{k+i} - \bar{x}_k) \\ &+ (\boldsymbol{u}_{k+i} - \bar{\boldsymbol{u}}_k)^T \boldsymbol{\Sigma} (\boldsymbol{u}_{k+i} - \bar{\boldsymbol{u}}_k), \\ \text{subj. to} \quad & x_{k+i+1} = a x_{k+i} + \boldsymbol{b}\boldsymbol{u}_{k+i} + b_d d_k, \\ & x_k = \hat{x}_k, \\ & d_k = \hat{d}_k, \\ & u_{k+1}(1) = 1, \\ & \boldsymbol{u}_{min} \le \boldsymbol{u}_{k+i} \le \boldsymbol{u}_{max}, \end{aligned} \tag{9}$$

where $\boldsymbol{U}$ is the input sequence $\boldsymbol{U} = [\boldsymbol{u}_k, ..., \boldsymbol{u}_{k+N-1}]$ within the prediction horizon N, q is a weighting factor and $\bar{x}$ and $\bar{\boldsymbol{u}}$ are the target state and target input vector, respectively. The MPC is designed to track these steady-state target values. The calculation of these target variables is discussed in the next section.

3.4 Target Calculation - The Minimum-Variance Approach

The aim of the target calculation is to find an input vector $\bar{\boldsymbol{u}}_k = [\bar{u}_{1|k}, \, \bar{u}_{2|k}]^T$ at time step k so that the target output $\bar{y}_k = \bar{x}_k$ meets the reference r_k in a steady state with minimized variance:

$$r_k = b_0 + b_1 \bar{u}_{1|k} + b_2 \bar{u}_{2|k} + d_k. \tag{10}$$

It can be seen that there is no unique solution for $\bar{u}_{1|k}$ and $\bar{u}_{2|k}$ so that (10) is fulfilled.

In this paper, we suggest incorporating knowledge about the model uncertainty to find a solution for the target inputs. The estimate for the parameter vector is given by

$$\hat{\boldsymbol{\theta}} = \begin{bmatrix} \hat{b}_0 & \hat{b}_1 & \hat{b}_2 \end{bmatrix}^T. \tag{11}$$

Moreover, the estimate for the parameter covariance matrix $\hat{\boldsymbol{\Sigma}}$ is assumed to be known. The undisturbed model output in a steady state can be written as

$$\hat{y} = \boldsymbol{u}^T \hat{\boldsymbol{\theta}}. \tag{12}$$

The output variance can be computed by

$$\begin{aligned} \text{Var}(\hat{y}) &= \text{E}\{(\hat{y} - y)^2\} \\ &= \text{E}\{(\boldsymbol{u}^T \hat{\boldsymbol{\theta}} - \boldsymbol{u}^T \boldsymbol{\theta})^2\} \\ &= \boldsymbol{u}^T \text{E}\{(\hat{\boldsymbol{\theta}} - \boldsymbol{\theta})(\hat{\boldsymbol{\theta}} - \boldsymbol{\theta})^T\} \boldsymbol{u} \\ &= \boldsymbol{u}^T \boldsymbol{\Sigma} \boldsymbol{u}. \end{aligned} \tag{13}$$

This output variance is taken as the cost function and is minimized to find the target input vector $\bar{\boldsymbol{u}}_k$ at time step k:

$$\begin{aligned} \min_{\boldsymbol{u}_k} J_{\text{target}} &= \boldsymbol{u}_k^T \hat{\boldsymbol{\Sigma}} \boldsymbol{u}_k, \\ \text{subj. to} \quad & \boldsymbol{u}_k(1) = 1, \\ & r_k = \hat{b}_0 + \hat{b}_1 \bar{u}_{1|k} + \hat{b}_2 \bar{u}_{2|k} + \hat{d}_k, \\ & \boldsymbol{u}_{min} \le \bar{\boldsymbol{u}}_k \le \boldsymbol{u}_{max}. \end{aligned} \tag{14}$$

The input constraints in the optimization problem (14) can cause infeasibility. This means that no input vector within the constraints exists so that the model output meets the reference in a steady state. In this case instead the squared steady-state difference between the output and its reference

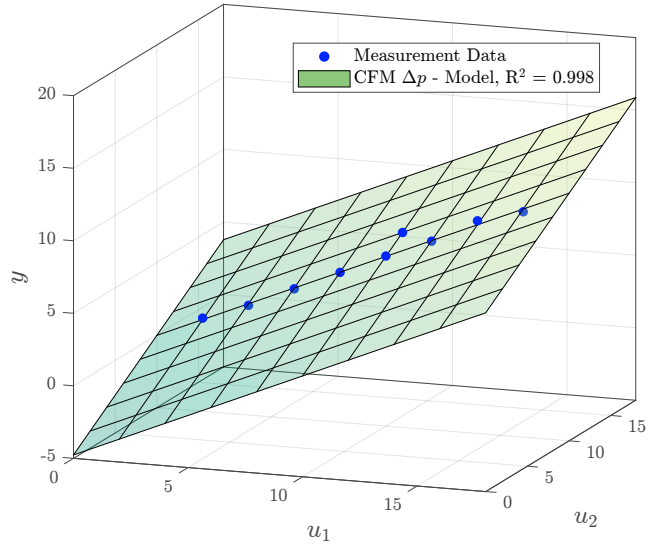

Fig. 2. Measurement points and model for Δp (model output y) as a function of the inputs $\dot{V}_p$ and $\dot{V}_s$.

$$(r_k - \boldsymbol{u}_k^T \hat{\boldsymbol{\theta}} + \hat{d}_k)^2 \tag{15}$$

is minimized by solving the quadratic program

$$\begin{aligned} \min_{\boldsymbol{u}_k} J_{\text{target}} &= \boldsymbol{u}_k^T \hat{\boldsymbol{\theta}} \hat{\boldsymbol{\theta}}^T \boldsymbol{u}_k - 2(r_k + \hat{d}_k)\boldsymbol{u}_k \boldsymbol{\theta} \\ \text{subj. to} \quad & \boldsymbol{u}_k(1) = 1 \\ & \boldsymbol{u}_{min} \leq \bar{\boldsymbol{u}}_k \leq \boldsymbol{u}_{max}. \end{aligned} \tag{16}$$

4. RESULTS AND DISCUSSION

An identification experiment to find a mathematical model describing the input-output relationships has been carried out at the CFM at TU Wien. The minimum variance MPC approach is tested in simulations and compared to an MPC which does not consider model uncertainties in its design, hereinafter referred to as *Standard MPC*. For this Standard MPC, the identity matrix is used instead of the covariance matrix $\boldsymbol{\Sigma}$ in the cost functions (9) and (14). Thus, the Standard MPC aims to minimize the norm of the input vector.

4.1 Plant Model

Carrying out identification experiments at DFB gasifiers is usually an expensive task. Although industrial plants are running continuously, they are typically operated at the same operating points. Thus, only for a small region of the input space measurement data is available. Our control concept is presented for the CFM, however, the aim is to apply it to a DFB gasifier. Therefore, we assume that only a small data set for system identification is available. Furthermore, we investigate the case that the quality of data is different for different input variables. Fig. 2 shows the data points as well as the identified steady-state model

$$y = -4.7660 + 0.67158u_1 + 0.47462u_2, \tag{17}$$

describing the bed material circulation. The estimated coefficients in (17) show that the first input u_1, the primary air, locally has a higher influence on the bed material circulation. Moreover, it can be seen in Fig. 2 that 8 operating points are available with different values in the first input u_1, the primary air volume flow. For the second input u_2, however, only 2 different data points are available. This leads to higher uncertainties for the parameter b_2 describing the influence of u_2 on the output. The ellipsoid in Fig. 3 shows the region in which the parameters are located with a probability of 95 %, described by the estimate of the parameter covariance matrix

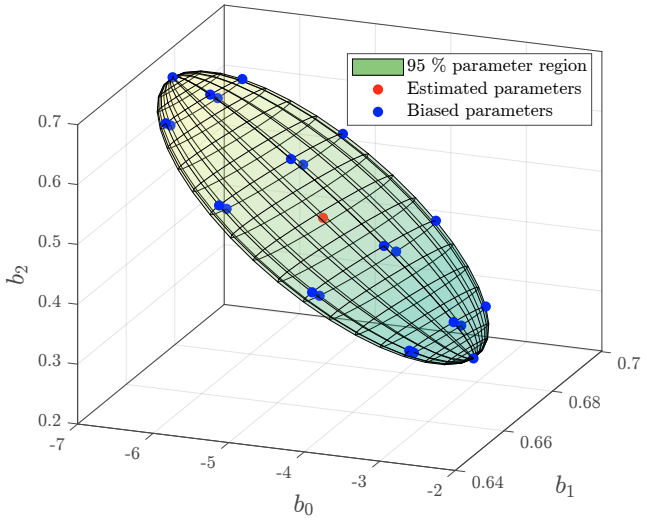

Fig. 3. The ellipsoid gives the region, where the parameters are located with a probability of 95 %. The red point shows the least squares estimate of the model parameters. The blue points are located on the ellipsoid and are used for closed-loop simulations.

$$\hat{\boldsymbol{\Sigma}} = \begin{bmatrix} 0.6974 & -5.611e-04 & -0.0675 \\ -5.611e-04 & 1.403e-04 & -7.013e-05 \\ -0.0675 & -7.013e-05 & 0.0067 \end{bmatrix}. \tag{18}$$

The center of the ellipsoid corresponds to the parameter estimate. The closed-loop simulations are done with different plant models, where the parameters are biased to simulate modeling inaccuracies. The blue points in Fig. 3 show the different parameter sets used for the plant models in the closed-loop simulations.

4.2 Circulation Control Without Input Constraints

As a first step, the MPC algorithm is tested without any input constraints. The MV-MPC requires only one parameter, the state weighting q in (9). This parameter is chosen to be $q = 10^{-2}$. No input weighting is necessary, since the estimated parameter covariance matrix $\hat{\boldsymbol{\Sigma}}$ is chosen as the input weighting in the MPC cost function. For the Standard MPC, the state weighting $q = 20$ and the input weighting matrix $\boldsymbol{R} = \boldsymbol{I}$ is chosen in the MPC cost function. With these weightings, both MPC algorithms cause the same response to a step in the reference, as long as there are no model inaccuracies considered in the simulation. For the Standard MPC, the computation of the target values is done by minimizing the norm of the input vector. The disturbance model and the observer design are

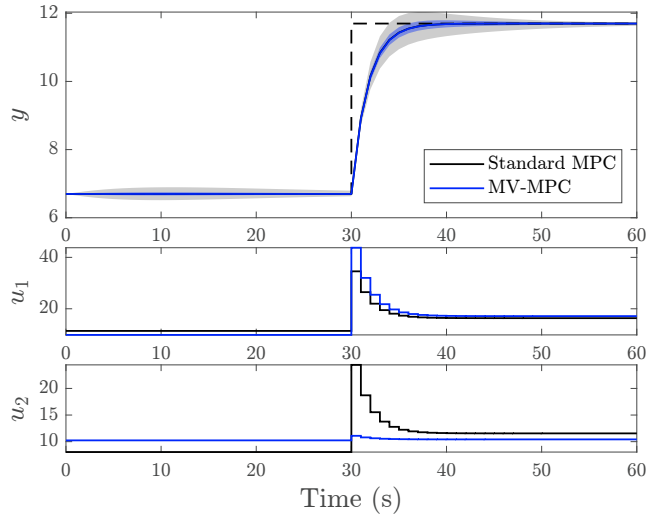

Fig. 4. Simulation of a step in the reference without input constraints.

the same for both MPCs. The Kalman gain matrix $\boldsymbol{L}$ is computed by solving the discrete-time algebraic Riccati equation, with the process noise covariance matrix $\boldsymbol{Q} = \boldsymbol{I}$, and the measurement noise variance $\boldsymbol{R} = 10^2$.

The closed-loop simulation is carried out with the original plant model and with 22 different plant models that are biased in their parameters. The upper part of Fig. 4 shows the response to a step in the reference. The solid lines show the simulation with an unbiased plant model, which results in the same response for the MV-MPC and the Standard MPC. The areas around the solid lines indicate where the output trajectories are located for the simulations with the biased plant models. It can be seen that for the MV-MPC approach the deviation from the design trajectory can be reduced. For the biased plant models, also before the step in the reference, a deviation from the reference can be observed since the necessary control input needs to be corrected using the disturbance model. However, for the MV-MPC the maximum deviation from the design trajectory before the step in the reference is around 0.05 mbar, therefore it can hardly be seen in the plot. Due to the disturbance model, offset-free reference tracking can be achieved with both MPCs in steady-state (Maeder et al. (2009)). In the lower part of the figure, the input trajectories are shown for the simulation with the unbiased plant models. It can be seen that the MV-MPC avoids the usage of the input u_2, since changes in this input would lead to a higher variance in the model output. The input trajectories are also shown in Fig. 5. In this figure, also the variance of the steady-state model output according to (13) is shown as a function of the input. As expected, the MV-MPC algorithm keeps the inputs in an area leading to low uncertainties in the model output.

4.3 Circulation Control With Input Constraints

For the second simulation scenario, input constraints are applied and a maximum value of 25 Nm^3/h is set as a constraint for both inputs. Simulations are again performed for the original and for biased plant models. Fig. 6 shows the closed-loop step response plot for the MV-MPC and the Standard MPC. Here, the output trajectories with the

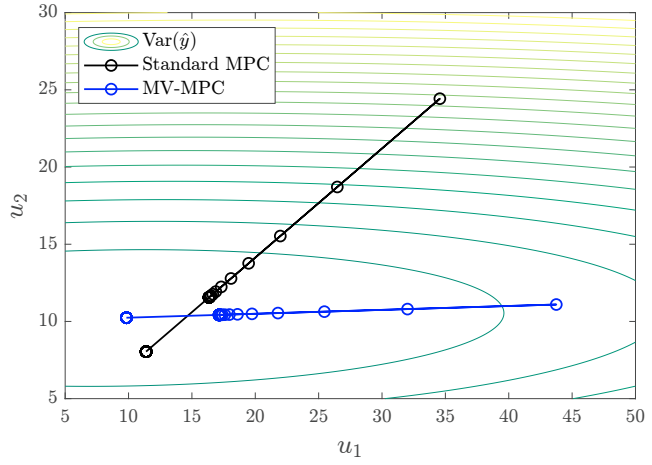

Fig. 5. MPC trajectories in the input space. The contour lines show the model output variance: brighter colors indicate a higher output variance and therefore a higher model uncertainty.

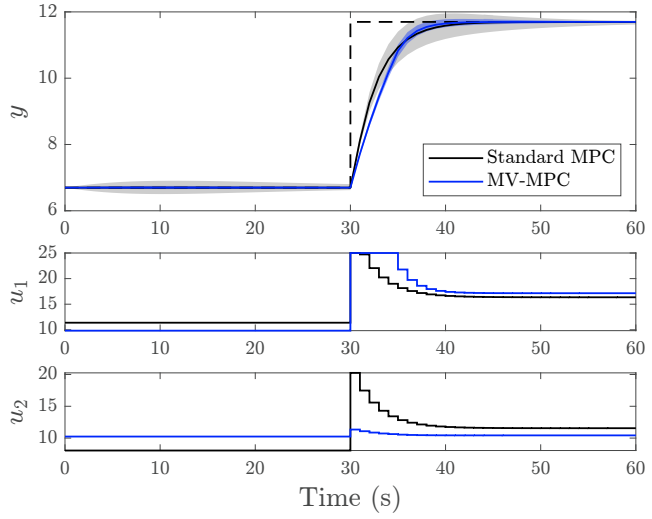

Fig. 6. Simulation of a step in the reference with input constraints. Both inputs are constrained to a maximum of 25 Nm^3/h.

unbiased plant model deviate for both MPCs, because the constraints are active for different time spans. Moreover, it can be seen that also with input constraints the MV-MPC reduces the deviation from the design trajectory if there are inaccurate parameters in the simulation model. Fig. 7 shows the input trajectories and the model output variance. Again, the MV-MPC keeps the inputs in an area with low model uncertainties.

Table 1 shows the maximum deviations from the design trajectory with the MV-MPC and the Standard MPC, both for the simulation without constraints and with constraints. With the MV-MPC the deviation can be reduced by up to 65.9 %.

5. CONCLUSION

In this paper, an MPC algorithm has been presented, which is beneficial for the case that there are known model uncertainties and redundant inputs for process control. In this case, the proposed MPC algorithm can improve

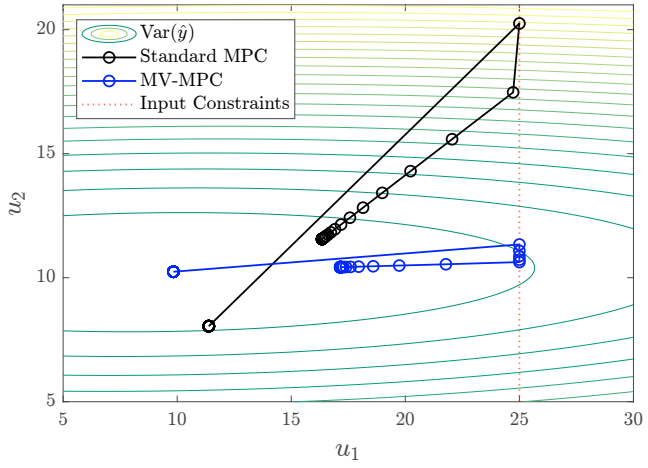

Fig. 7. Input Trajectory.

Table 1. Maximum deviation from the design trajectory.

	Standard MPC	MV-MPC	Δ
without constraints	0.5005 mbar	0.1705 mbar	-65.94 %
with constraints	0.4756 mbar	0.1868 mbar	-60.72 %

the closed-loop performance. This can be advantageous when system identification is expensive and there are high inaccuracies in the parameter estimates, which is often the case for DFB plants. The deviation from the reference can then be reduced and the bed material circulation demanded by the plant operator can be achieved more rapidly. Input constraints can be explicitly considered by the algorithm. An implementation of the proposed algorithm to the 100 kW pilot plant is envisaged.

REFERENCES

Benedikt, F., Schmid, J.C., Fuchs, J., Mauerhofer, A.M., Müller, S., and Hofbauer, H. (2018). Fuel flexible gasification with an advanced 100 kW dual fluidized bed steam gasification pilot plant. *Energy*, 164, 329–343. doi: 10.1016/j.energy.2018.08.146.

Fonseca, R.R., Schmitz, J.E., Fileti, A.M.F., and Da Silva, F.V. (2013). A fuzzy–split range control system applied to a fermentation process. *Bioresource Technology*, 142, 475–482. doi:10.1016/J.BIORTECH.2013.05.083.

Fuchs, J., Schmid, J., Benedikt, F., Mauerhofer, A., Muller, S., and Hofbauer, H. (2018). A general method for the determination of the entrainment in fluidized beds. *The International Journal of Multiphysics*, 12(4), 359–372. doi:10.21152/1750-9548.12.4.359.

Fuchs, J. (2013). *Ermittlung des Betriebskennfeldes einer innovativen Zweibett-wirbelschicht anhand von Kaltmodelluntersuchungen*. University of Leoben.

Grauer, J.A. and Pei, J. (2021). Minimum-Variance Control Allocation Considering Parametric Model Uncertainty. In *AIAA SCITECH 2022 Forum*, AIAA SciTech Forum. American Institute of Aeronautics and Astronautics. doi:10.2514/6.2022-0749.

Johansen, T.A. and Fossen, T.I. (2013). Control allocation—A survey. *Automatica*, 49(5), 1087–1103. doi:10.1016/J.AUTOMATICA.2013.01.035.

Kraft, S., Kirnbauer, F., and Hofbauer, H. (2017). CPFD simulations of an industrial-sized dual fluidized bed steam gasification system of biomass with 8 MW fuel input. *Applied Energy*, 190, 408–420. doi: 10.1016/J.APENERGY.2016.12.113.

Liu, H., Cattolica, R.J., and Seiser, R. (2016). CFD studies on biomass gasification in a pilot-scale dual fluidized-bed system. *International Journal of Hydrogen Energy*, 41(28), 11974–11989. doi: 10.1016/J.IJHYDENE.2016.04.205.

Lunzer, A., Kraft, S., Müller, S., and Hofbauer, H. (2021). CPFD simulation of a dual fluidized bed cold flow model. *Biomass Conversion and Biorefinery*, 11(1), 189–203. doi:10.1007/s13399-020-01229-4.

Maeder, U., Borrelli, F., and Morari, M. (2009). Linear offset-free Model Predictive Control. *Automatica*, 45(10), 2214–2222. doi: 10.1016/j.automatica.2009.06.005.

Matsuda, S. (2008). Measurement of solid circulation rate in a circulating fluidized bed. *Powder Technology*, 187(2), 200–204. doi:10.1016/J.POWTEC.2008.02.004.

Medrano, J.A., Nordio, M., Manzolini, G., van Sint Annaland, M., and Gallucci, F. (2016). On the measurement of solids circulation rates in interconnected fluidized beds: Comparison of different experimental techniques. *Powder Technology*, 302, 81–89. doi: 10.1016/J.POWTEC.2016.08.035.

Nigitz, T., Gölles, M., Aichernig, C., Schneider, S., Hofbauer, H., and Horn, M. (2020). Increased efficiency of dual fluidized bed plants via a novel control strategy. *Biomass and Bioenergy*, 141, 105688. doi: 10.1016/J.BIOMBIOE.2020.105688.

Pröll, T. and Hofbauer, H. (2010). Process and device for providing a constant product gas rate from a fluidized bed gas generation plant.

Reyes-Lúa, A. and Skogestad, S. (2020). Multi-input single-output control for extending the operating range: Generalized split range control using the baton strategy. *Journal of Process Control*, 91, 1–11. doi: 10.1016/J.JPROCONT.2020.05.001.

Shrestha, S., Ali, B.S., and Binti Hamid, M.D. (2016). Cold flow model of dual fluidized bed: A review. *Renewable and Sustainable Energy Reviews*, 53, 1529–1548. doi:10.1016/J.RSER.2015.09.034.

Stanger, L., Schirrer, A., Benedikt, F., Bartik, A., Jankovic, S., Müller, S., and Kozek, M. (2023). Dynamic modeling of dual fluidized bed steam gasification for control design. *Energy*, 265, 126378. doi: 10.1016/J.ENERGY.2022.126378.

Stollhof, M., Penthor, S., Mayer, K., and Hofbauer, H. (2018). Estimation of the solid circulation rate in circulating fluidized bed systems. *Powder Technology*, 336, 1–11. doi:10.1016/J.POWTEC.2018.05.033.